F. T. DODGE
Senior Research Engineer.
Assoc. Mem. ASME

L. R. GARZA
Research Engineer.

Department of Mechanical Sciences,
Southwest Research Institute,
San Antonio, Texas

Experimental and Theoretical Studies of Liquid Sloshing at Simulated Low Gravity[1]

Analyses and experimental comparisons are given for liquid sloshing in a rigid cylindrical tank under conditions of moderately small axial accelerations; in particular, the theory is valid for Bond numbers larger than 10. The analytical results are put in the form of an equivalent mechanical model, and it is shown that the sloshing mass and the natural frequency of the first mode, for a liquid having a 0 deg contact angle at the tank walls, are smaller than for high-g conditions. The experimental data, obtained by using several small-diameter tanks and three different liquids, are compared to the predictions of the mechanical model; good correlation is found in most cases for the sloshing forces and natural frequency as a function of Bond number.

Introduction

THE FREE surface wave motion, or sloshing, of liquid fuel in large rocket boosters is a well-recognized problem in technology. Results are available for lateral sloshing [1, 2],[2] nonlinear aspects [3], vertical sloshing, i.e., sloshing in which the excitation of the tank is in the axial direction [4, 5], and other phenomena [6]. Nearly all the experimental and theoretical work has been limited, however, to situations in which the steady axial acceleration of the tank (gravity or thrust or both) is large; thus the liquid's motion can be determined by considering only the body forces in the liquid and the forces arising at the walls of the tank. But there are occasions when the axial acceleration is small, as for example, when the booster is coasting in an earth orbit, and then other forces must be taken into account; the most important of these forces is usually the interfacial tension between the liquid fuel and the ullage gas. The resulting free surface motion under such conditions is called "low-gravity" sloshing.

Most of the previous research on low-gravity fluid mechanics is reviewed in [7], which also contains a lengthy reference list. The reports by Reynolds and his co-workers [8, 9] are especially recommended. Some recent work is given in [10, 11]. However, to the authors' knowledge, there are no experimental or explicit theoretical results available for the important problem of sloshing during forced excitation of the tank (although the generalized analysis of [10] supposedly can be specialized to include this). In particular, there is a complete lack of experimental data for the dynamic forces exerted by the sloshing liquid. Thus, in this paper, analytical and experimental results for low-gravity sloshing in a rigid cylindrical tank are presented for the case of simple harmonic translation of the tank.

Experimental data for low-gravity sloshing are not obtained easily. Laboratory facilities that can duplicate an actual small axial acceleration, such as drop towers, are usually not able to provide the low-gravity field for a sufficiently long duration to get consistent and reliable sloshing data. An alternative method of *simulating* low gravity is to use models of small dimensions; in this way, the interfacial or capillary forces can be made comparable to, or greater than, the gravity or body forces even in the standard gravity field; thus this is a suitable "low-gravity" test for some purposes. The available test time is not a problem with this kind of simulation, but the liquid motion and the slosh forces are very small because of the smallness of the model tank. In the experiments reported here, the simulation was accomplished through this use of small models; such a simulation required that an extremely sensitive and precise dynamometer system be constructed since slosh forces on the order of 0.0001 lb were expected. As far as is known to the authors, the data presented here are the first, and the only up to now, that give sloshing forces and frequencies for low gravitational (i.e., small Bond number) conditions. (However, some data for natural frequencies have been published previously [9].)

The Bond numbers ($N_{BO} = \rho g R_0^2/T$ is an indication of the size of body forces relative to interfacial forces[3]) used in the tests were in the range of 10 to 100. Now, very low-gravity fluid mechanics are characterized by $N_{BO} < 1$ while high-g problems occur for

[1] The results presented in this paper were obtained during the course of research sponsored by the NASA Marshall Space Flight Center under Contract NAS8-20290.

[2] Numbers in brackets designate References at end of paper.

Contributed by the Applied Mechanics Division and presented at the Applied Mechanics Conference, Pasadena, Calif., June 26–28, 1967, of THE AMERICAN SOCIETY OF MECHANICAL ENGINEERS.

Discussion of this paper should be addressed to the Editorial Department, ASME, United Engineering Center, 345 East 47th Street, New York, N. Y. 10017, and will be accepted until October 15, 1967. Discussion received after the closing date will be returned. Manuscript received by ASME Applied Mechanics Division, November 14, 1966. Paper No. 67—APM-14.

[3] See Nomenclature for definition of symbols.

Nomenclature

NOTE: Symbols in parentheses are the nondimensional equivalents of the preceding quantity.

a_n = expansion coefficient in series for Φ; see equation (9)
b_n = expansion coefficient in series for ϵ; see equation (10)
$C1_{nm}$, $C2_{nm}$, $C3_{nm}$ = Fourier-Bessel coefficients in equations (11) and (12)
$f(F)$ = height of meniscus above $Z = 0$; see Fig. 1
F_L = lateral force exerted on tank by liquid
g = steady axial acceleration or gravity
$J_1(\lambda_n R)$ = first-order Bessel function of first kind
M = number of terms in series for Φ and ϵ, or number of slosh masses
N_{BO} = Bond number, $\rho g R_0^2/T$
$r(R)$, θ, $z(Z)$ = axes of tank-fixed coordinate system; see Fig. 1
$t(\tau)$ = time
T = interfacial tension
$x_0(X_0)$ = excitation amplitude
β = nondimensional meniscus height at tank wall
ζ = total wave height above $Z = 0$; see Fig. 1
$\eta(\epsilon)$ = wave height above meniscus; see Fig. 1
λ_n = roots of $J_1'(\lambda_n) = 0$
ρ = density of liquid
$\phi(\Phi)$ = velocity potential
Ω_n = dimensionless natural frequency of nth mode
$\omega(\Omega)$ = excitation frequency

$N_{BO} > 1000$. Thus $10 < N_{BO} < 100$ should be classified as moderately low-gravity problems; Bond numbers of this size, for example, are encountered in coasting orbits of some large rocket boosters where the effective axial acceleration is only about 2×10^{-5} of standard gravity [12]. Even though body forces are still dominant, but not overwhelmingly so, for $10 < N_{BO} < 100$, interfacial tension causes the undisturbed free surface to depart considerably from the usual flat surface and, hence, interfacial curvature and forces must be included in the analysis.

Analysis

Effects such as stratification or thermally driven motions are ignored in the analysis and are absent in the experiments. The influence of viscosity is also neglected in the analysis since experience has shown it to be small and accountable for a posteriori by adding suitable linear damping. In other words, the usual sloshing assumptions are made: Incompressible, ideal liquid; irrotational motions; negligible inertia of the ullage gas. An r, θ, z cylindrical coordinate system is *fixed* to the tank and centered along the axis at the point it intersects the undisturbed free surface, as shown in Fig. 1. The depth of liquid below $z = 0$ is taken to be so large that the tank bottom is essentially at $z = -\infty$; this greatly simplifies the algebraic labor and is valid if $h/2R_0 > 1$. The height, $f(r)$, of the undisturbed, axisymmetric free surface is measured positively above $z = 0$, and the wave height $\eta(r, \theta, t)$ is then measured from this surface and not from $z = 0$.

A velocity potential $\phi(r, \theta, z, t)$ is defined such that the liquid's velocity relative to the tank is $\mathbf{V} = \nabla\phi$. The equations are immediately made nondimensional by dividing all quantities having the dimensions of length by R_0 and those having the dimensions of time by $(R_0/g)^{1/2}$; for example, the nondimensional wave height is $\epsilon(R, \theta, \tau) = \eta(r/R_0, \theta, t\sqrt{g/R_0})/R_0$ and the nondimensional frequency is $\Omega = \omega(R_0/g)^{1/2}$.[4] Furthermore, the nonlinear boundary conditions at the free surface are linearized by assuming that Φ and ϵ are small compared to unity; note that this does *not* imply that the equilibrium shape $f(r)$ need be nearly plane. The complete set of nonlinear equations could probably be solved by methods similar to those outlined in [3], or by Hutton [13], or by Dodge, et al. [5], but a nonlinear analysis is not usually warranted in applications and, in addition, a linear analysis serves to point out the main differences between low-gravity sloshing and the usual high-g sloshing.

[4] For very small Bond numbers, a better nondimensionalization of time is obtained by using $(\rho R_0^3/T)^{1/2}$ as the significant time. This avoids any difficulties that might arise as $g \to 0$.

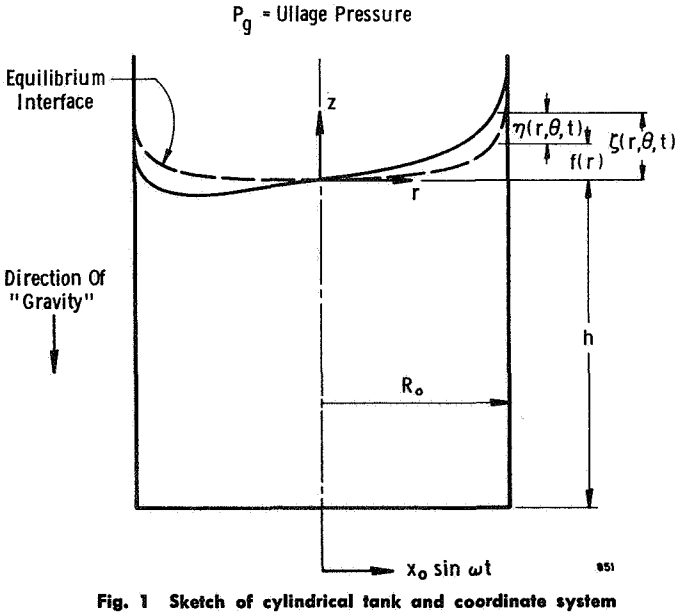

Fig. 1 Sketch of cylindrical tank and coordinate system

The potential must satisfy Laplace's equation

$$\nabla^2\Phi = 0 \text{ in the liquid} \tag{1}$$

and two conditions at the tank boundaries

$$\partial\Phi/\partial R = 0, \qquad R = 1 \tag{2}$$

$$\partial\Phi/\partial Z = 0, \qquad Z = -\infty \tag{3}$$

The first integral of the equations of motion evaluated just below the free surface gives one relation between the velocity potential and the wave height; another condition is obtained by requiring that the normal pressure across the free surface must be discontinuous by an amount proportional to the product of the interfacial tension and the mean surface curvature. By combining these two equations and linearizing with respect to Φ and ϵ, as shown in [16], one relation results:

$$\frac{\partial\Phi}{\partial\tau} + \epsilon - \frac{1}{N_{BO}}\left(\frac{1}{R}\frac{\partial}{\partial R}\left\{\frac{R\dfrac{\partial\epsilon}{\partial R}}{\left[1+\left(\dfrac{dF}{dR}\right)^2\right]^{3/2}}\right\} + \frac{1}{R^2}\frac{\partial}{\partial\theta}\left\{\frac{\dfrac{\partial\epsilon}{\partial\theta}}{\left[1+\left(\dfrac{dF}{dR}\right)^2\right]^{1/2}}\right\}\right) - X_0\Omega^2 R\cos\theta\sin\Omega\tau = 0, \qquad Z = F \tag{4}$$

A second condition between the potential and the wave height arises from the fact that the motion of the free surface and the fluid velocity at the surface must be consistent with each other; linearized, this condition is

$$\frac{\partial\epsilon}{\partial\tau} - \frac{\partial\Phi}{\partial Z} + \frac{dF}{dR}\left(\frac{\partial\Phi}{\partial R}\right) = 0, \qquad Z = F \tag{5}$$

The final requirement for a well-posed problem is knowledge of the angle at which the free surface meets the tank walls.[5] It is assumed here that the contact angle measured in the liquid, for the undisturbed surface, is zero, which is typical of several existing fuel-tank systems. However, it is entirely possible that the angle at which the moving wave meets the wall is not the same as the static contact angle; this phenomenon is known as contact angle hysteresis. Some researchers have tried to account for the hysteresis by assuming that

$$\partial\epsilon/\partial R = C_1\epsilon, \qquad R = 1 \qquad Z = F(1)$$

which seems to imply that the change in the contact angle depends only on the distance the free surface is displaced from equilibrium. If C_1 is truly a constant, this equation does not seem able to explain the damping or energy dissipation caused by the hysteresis. The entire subject of contact angle hysteresis and surface wave damping has recently been reviewed by Miles [14], and he points out that the important physical processes are far from being fully understood. Thus, rather than postulate an arbitrary functional relationship, hysteresis is neglected in the analysis, and the contact line is assumed to slide easily along the tank walls—the so-called "free edge" condition. In other words, the contact angle condition used here is

$$\partial\epsilon/\partial R = 0, \qquad R = 1 \qquad Z = F(1) \tag{6}$$

Since the contact angle is defined by

$$\theta_c = \cot^{-1}\left\{\frac{\partial\zeta}{\partial r}\Big/\left[1+\left(\frac{\partial\zeta}{r\partial\theta}\right)^2\right]^{1/2}\right\}$$

(at $r = R_0$), equation (6) actually implies that θ_c is always equal

[5] In high-g analyses, the free surface is flat at equilibrium and is assumed to deform to whatever shape the dynamics require, regardless of the value of the contact angle.

to zero in the linearized approximations used here.[6]

It is clear that the equilibrium free surface shape, $F(R)$, must be known before an analysis of the sloshing can be completed. Exact computations of $F(R)$ can be quite involved [10] but, fortunately, very good approximate expressions can be derived for the range of Bond numbers of interest here. For $N_{BO} \ll 1$, the equilibrium interface is nearly spherical; that is, $F(R) = 1 - (1 - R^2)^{1/2}$. As N_{BO} increases, the interface becomes flatter. Using this as a guide, Satterlee and Chin [15] showed that a modified spherical shape, $F(R) = \beta[1 - (1 - R^2)^{1/2}]$ with β a function of N_{BO}, was an approximate solution of the equations that agreed well with experiments and exact solutions for $N_{BO} < 10$. For large N_{BO}, the assumed shape, however, was not "flat" enough. Thus, for $10 < N_{BO} < 100$, a reasonable assumption is

$$F(R) = \beta[1 - (1 - R^2)^{1/2}] \tag{7}$$

since the curvature of this is considerably less than that of the modified spherical shape. Equation (7) already satisfies the boundary conditions that $F(0) = dF(0)/dR = 0$ and $dF(1)/dR = \cot \theta_c = \infty$; by substituting it into the equilibrium analog of equation (4), it can be seen that equation (7) also satisfies the correct interface curvature-pressure relation at $R = 0$. Thus reasonable predictions of β, the nondimensional height of the meniscus at the tank wall, can be obtained by forcing equation (7) to satisfy this relation at $R = 1$. Doing this gives the result:

$$\beta^2 N_{BO} - \beta^2 - (2/3) = 0 \tag{8}$$

Equations (7) and (8) agree fairly well with the experimental data of [15] for $N_{BO} > 10$.

Even after linearizing the equations and assuming a relatively simple expression for $F(R)$, the authors know of no function or set of functions that will exactly satisfy all of equations (1–6). Of several approximate methods, the one selected here is to construct a solution from the known set of functions for sloshing when $N_{BO} = \infty$, i.e., $F = 0$. This seems logical because body forces are still the largest forces when $N_{BO} > 10$. Thus it is assumed that the velocity potential is

$$\Phi(R, \theta, Z, \tau) = \sum_{n=1}^{\infty} a_n(\tau) \cdot J_1(\lambda_n R) \cdot \cos \theta \cdot e^{\lambda_n Z} \tag{9}$$

and the wave shape is

$$\epsilon(R, \theta, \tau) = \sum_{n=1}^{\infty} b_n(\tau) \cdot J_1(\lambda_n R) \cdot \cos \theta \tag{10}$$

These two series expansions will identically satisfy equations (1), (2), (3), and (6) if λ_n are the roots of $J_1'(\lambda_n) = 0$. This will also insure that each $J_1(\lambda_n R)$ is orthogonal to all the rest in the interval $0 \leq R \leq 1$, with the weighting function equal to R. (Note, however, that the expansion for ϵ cannot be made to satisfy a contact line condition of the form $\partial\epsilon/\partial R = C_1\epsilon$ if $C_1 \neq 0$.)

Now equations (9) and (10) are substituted into the boundary conditions, equations (4) and (5), in order to determine the a_n and b_n. The resulting two equations are then expanded again into a Bessel-Fourier series of $J_1(\lambda_m R) \cos \theta$ terms. The results for equation (5) are

$$\sum_{n=1}^{\infty} \left\{ \dot{b}_n + \sum_{m=1}^{\infty} C1_{nm} a_m \right\} J_1(\lambda_n R) \cos \theta = 0 \tag{11}$$

and for equation (4)

$$\sum_{n=1}^{\infty} \left\{ b_n + \sum_{m=1}^{\infty} C2_{nm} \dot{a}_m + \sum_{m=1}^{\infty} C3_{nm} b_m - \frac{2X_0\Omega^2}{(\lambda_n^2 - 1)J_1(\lambda_n)} \sin \Omega\tau \right\} J_1(\lambda_n R) \cos \theta = 0 \tag{12}$$

where the superscript dots indicate time differentiation, and $C1_{nm}$, $C2_{nm}$, and $C3_{nm}$ are the functions of β and N_{BO} given in the Appendix. After combining these two equations to eliminate the $b_n(\tau)$ and noting that each term in the sum over n must be identically zero, the resulting equations for the $a_n(\tau)$ are

$$\sum_{m=1}^{\infty} C2_{nm} \ddot{a}_m - \sum_{m=1}^{\infty} C1_{nm} a_m - \sum_{s=1}^{\infty} \left(C3_{ns} \sum_{m=1}^{\infty} C1_{sm} a_m \right) = \frac{2X_0\Omega^2}{(\lambda_n^2 - 1)J_1(\lambda_n)} \cos \Omega\tau = 0 \qquad n = 1, 2, 3, \ldots \tag{13}$$

It follows that each a_n depends on all the rest. Adequate results, nonetheless, can be obtained for the first few modes by truncating the equations at, say, $n = m = M$ and then solving the set of equations by ordinary methods.

Only the steady-state response is desired, so, by letting $a_n = A_n \cos \Omega\tau$ and substituting this into equation (13) (after truncating at $n = m = M$), the A_n can be calculated:

$$A_n = \left[\frac{K_{1n}\Omega^{2M} + K_{2n}\Omega^{2M-2} + \ldots + K_{Mn}\Omega^2}{\Omega^{2M} + K_1\Omega^{2M-2} + \ldots + K_{M-1}\Omega^2 + K_M} \right] X_0\Omega, \qquad n = 1, 2, \ldots, M \tag{14}$$

K_{ij} and K_i are various products of the constants in equations (13). Equation (14) can be put into a more revealing form by rearranging it according to the ideas of partial fractions:

$$A_n = \left[\frac{P_{1n}}{\Omega^2 - \Omega_1^2} + \frac{P_{2n}}{\Omega^2 - \Omega_2^2} + \ldots + \frac{P_{Mn}}{\Omega^2 - \Omega_M^2} \right] X_0\Omega^3, \qquad n = 1, 2, \ldots, M \tag{15}$$

The Ω_i^2, which are the factors of the denominator in equation (14), can be identified as the square of the natural frequency of the ith sloshing mode. They are ordered such that $\Omega_1^2 < \Omega_2^2 < \ldots < \Omega_M^2$. Physical reasoning implies that all the $\Omega_i^2 > 0$, and this turns out always to be the case.

By substituting these results in equation (9) and rearranging the terms according to natural frequency, the velocity potential works out to be

$$\Phi = X_0\Omega^3 \cos \theta \cos \Omega\tau \sum_{n=1}^{M} \frac{1}{\Omega^2 - \Omega_n^2} \times \left\{ \sum_{m=1}^{M} P_{nm} J_1(\lambda_m R) e^{\lambda_m Z} \right\} \tag{16}$$

The sum in braces in this equation is the normal mode function of the nth sloshing mode. Note that the index n in P_{nm} in equation (16) occupies the first position in the subscript while, in equation (15), it occupies the second; thus all the A_n contribute to each mode of Φ.

Similarly, by letting $b_n = B_n \sin \Omega\tau$, the wave shape is found to be

$$\epsilon = X_0\Omega^2 \cos \theta \sin \Omega\tau \sum_{n=1}^{M} \frac{1}{\Omega^2 - \Omega_n^2} \left\{ \sum_{m=1}^{M} Q_{nm} J_1(\lambda_m R) \right\} \tag{17}$$

where the Q_{ij} are various products of the P_{ij} and the constants in equation (11).[7]

The velocity potential and the wave shape have now been determined. Any particular sloshing mode can be studied by picking out the appropriate terms in equations (16) and (17); as will be seen, this is of considerable value in formulating an equivalent mechanical model. It should be emphasized that, once $C1_{nm}$, $C2_{nm}$, and $C3_{nm}$ are obtained by numerical integration with a computer, the remaining computations can be done by hand or with a desk calculator (at least as long as $M \leq 4$, which appears to be sufficient to give adequate results for the first

[6] $\zeta = f + \eta$, and so $(\partial\zeta/r\partial\theta)^2 = (\partial\eta/r\partial\theta)^2$, which may be neglected in comparison to unity. Also $\partial\zeta/\partial r = df/dr + \partial\eta/\partial r = df/dr$ at $r = R_0$, according to equation (6). Therefore, $\theta_c = \cot^{-1}(df/dr) = 0$ always.

[7] More complete details of the analysis and some numerical examples are given in [16]; they are omitted here for the sake of brevity.

mode). This is possibly an advantage not available with some other computation schemes.

Equivalent Mechanical Model

The sloshing characteristics important in missile applications (natural frequencies and forces and moments exerted on the tank) are displayed in a convenient form by an equivalent (mathematical) mechanical model. The proposed model for low-g sloshing is shown in Fig. 2; it is outwardly similar to models for high-g sloshing [1]. One spring-mass oscillator is included for each of the M slosh modes. The parameters of the model (m_0, m_n, h_0, h_n, k_n) are computed by matching the actual sloshing forces and moments with the forces and moments caused by the model for the same excitation.

The interfacial tension force acting on the tank walls along an element ds of the contact line is shown in Fig. 3; this force arises as a consequence of considering the interfacial tension to act similarly to a stretched membrane. $F_T = TR_0 d\theta$ is the linearized force in the plane of the wall (for a 0 deg contact angle) and the part of it acting in the increasing θ-direction is $F_{T,\theta} = F_T(\partial\eta/\partial\theta)$. The net force on the tank due directly to interfacial tension is a vertical force, not important here, and the vector sum of the $F_{T,\theta} \cdot ds$ forces, which turns out only to have a resultant in the direction of the tank excitation. Thus

$$F_1 = \int_0^{2\pi} -\frac{\partial\eta(r = R_0)}{\partial\theta} T \sin\theta d\theta = \left(\frac{1}{N_{BO}}\right) \times \pi\rho R_0^3 x_0\omega^2 \sin\omega t \sum_{n=1}^{M} \frac{H_n \frac{g}{R_0}}{\omega^2 - \Omega_n^2 \frac{g}{R_0}} \quad (18)$$

where $H_n = \sum_{m=1}^{M} Q_{nm} J_1(\lambda_m)$ is the dimensionless wave height at the wall for the nth mode.

The part of the force on the tank attributable directly to the liquid's motion can be calculated with the aid of Φ if a velocity potential for particles moving with the tank, $\Phi' = X_0\Omega R \cos\theta \times \cos\Omega\tau$, is added to it in order to make it valid in an inertia reference frame. Thus this part of the force is

$$F_2 = \rho g R_0^3 \int_0^{2\pi} \int_{-\frac{h}{R_0}}^{\beta+\epsilon_0} -\left[\frac{\partial\Phi(R = 1)}{\partial\tau} - X_0\Omega^2 \cos\theta \sin\Omega\tau + Z\right] \cos\theta dZ d\theta \quad (19)$$

where $\epsilon_0 = \epsilon(R = 1, \theta, \tau)$. The last term in the integral, the part equal to Z, is negligible for very large Bond numbers and, in such cases, the upper limit on the Z-integration is zero;[3] in this case, though, it has a nonnegligible part after linearization:

$$\int_0^{2\pi} \int_{-\frac{h}{R_0}}^{\beta+\epsilon_0} Z \cos\theta dZ d\theta = \beta \int_0^{2\pi} \epsilon_0 \cos\theta d\theta = \pi\beta X_0\Omega^2 \sin\Omega\tau \sum_{m=1}^{M} \frac{H_n}{\Omega^2 - \Omega_n^2} \quad (20)$$

Hence the force F_2 works out to be

$$F_2 = \pi\rho R_0^3 x_0\omega^2 \sin\omega t \left\{\beta + \frac{h}{R_0} - \beta \sum_{n=1}^{M} \frac{H_n \frac{g}{R_0}}{\omega^2 - \Omega_n^2 \frac{g}{R_0}} + \omega^2 \sum_{n=1}^{M} \frac{I_n}{\omega^2 - \Omega_n^2 \frac{g}{R_0}}\right\} \quad (21)$$

[3] That is, retaining the upper limit equal to ϵ_0 results only in higher-order terms in ϵ_0, which must eventually be discarded.

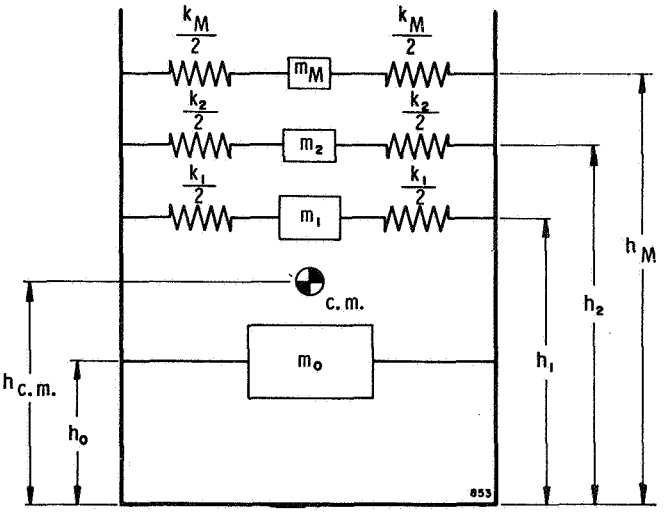

Fig. 2 Schematic of equivalent mechanical model

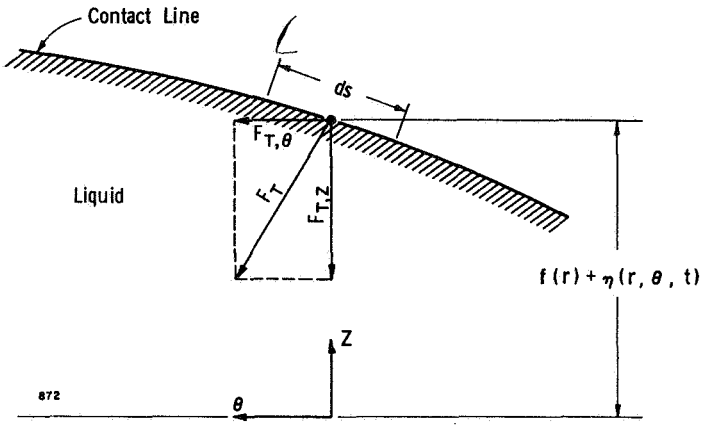

Fig. 3 Interfacial tension force at liquid-tank contact line

where $I_n = \sum_{m=1}^{M} \frac{P_{nm}}{\lambda_m} J_1(\lambda_m) e^{\lambda_m\beta}$. Now, combining F_1 and F_2 and rearranging various terms, the total lateral force on the tank is

$$F_L = \pi\rho R_0^3 x_0\omega^2 \sin\omega t \left\{\frac{h}{R_0} + \left[\beta + \left(\beta - \frac{1}{N_{BO}}\right) \sum_{n=1}^{M} \frac{H_n}{\Omega_n^2}\right] + \omega^2 \sum_{n=1}^{M} \frac{I_n - \left(\beta - \frac{1}{N_{BO}}\right) \frac{H_n}{\Omega_n^2}}{\omega^2 - \Omega_n^2 \frac{g}{R_0}}\right\} \quad (22)$$

By calculating the lateral force on the tank walls exerted by the system of masses and springs in the mechanical model, one finds

$$F_{\text{model}} = x_0\omega^2 \sin\omega t \left[m_0 + \sum_{n=1}^{M} m_n - \omega^2 \sum_{n=1}^{M} \frac{m_n}{\omega^2 - \frac{k_n}{m_n}}\right] \quad (23)$$

Comparing equations (22) and (23) shows that the mechanical model will give forces equivalent to the sloshing if

$$m_n = -\left[I_n - \left(\beta - \frac{1}{N_{BO}}\right) \frac{H_n}{\Omega_n^2}\right] \quad (24)$$

$$k_n/m_n = \Omega_n^2 (g/R_0) \quad (25)$$

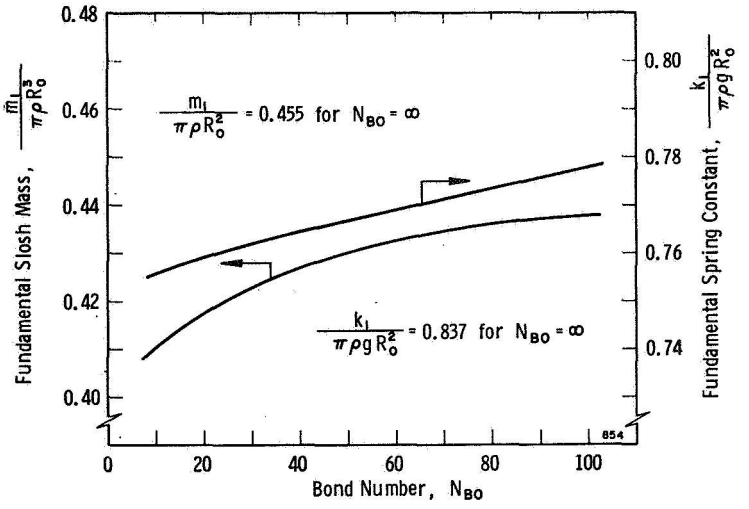

Fig. 4 Fundamental slosh mass and spring constant

and

$$m_0 + \sum_{n=1}^{M} m_n = \pi\rho R_0^3 \left[\frac{h}{R_0} + \beta + \left(\beta - \frac{1}{N_{BO}}\right) \sum_{n=1}^{M} \frac{H_n}{\Omega_n^2}\right] \tag{26}$$

Numerical calculations show that $\pi\rho R_0^3\left[\frac{h}{R_0} + \beta + \left(\beta - \frac{1}{N_{BO}}\right) \times \sum_{n=1}^{M} \frac{H_n}{\Omega_n^2}\right]$ is always very nearly equal to the total mass of the liquid, which is $m_T = \rho\pi R_0^3(h/R_0 + 0.264\beta)$; as $M \to \infty$, it is reasonable to assume that it would equal the liquid mass exactly (it would be surprising if it didn't), although this would probably be difficult to prove in complete generality. Assuming, then, that the term *is* equal to m_T, equation (26) shows that

$$m_0 + \sum_{n=1}^{M} m_n = m_T = \rho\pi R_0^3(h/R_0 + 0.264\beta) \tag{26'}$$

According to these equations, m_n and k_n can be computed from knowledge of only the nth sloshing mode and surface wave; i.e., the modes are not coupled. In Fig. 4, the fundamental sloshing mass m_1 and the fundamental spring constant k_1 are shown as functions of the Bond number. In every case, the amount of liquid participating in the sloshing motion is smaller than for $N_{BO} = \infty$; and, in fact, for $N_{BO} = 10$, the sloshing mass is almost 10 percent less than the high-g case. The amount of liquid participating in the second and higher modes is very small.

Carrying out the same kind of comparisons between the sloshing moment on the tank and the model moment results in the same values for m_0, m_n, and k_n; and, in addition, it is required that

$$h_n = R_0\left\{\frac{h}{R_0} - \frac{1}{\Omega_n^2} - \frac{\pi\rho R_0^3}{m_n}\left[\sum_{m=1}^{M}\left(\beta - \frac{1}{\lambda_m}\right) \times \frac{P_{nm}J_1(\lambda_m)e^{\lambda_m\beta}}{\lambda_m} - \beta\left(\beta - \frac{1}{N_{BO}}\right)\frac{H_n}{\Omega_n^2}\right]\right\} \tag{27}$$

and

$$h_0 = \frac{1}{m_0}\left(m_T h_{c.m.} - \sum_{n=1}^{M} m_n h_n\right) \tag{28}$$

where the center-of-mass coordinate above the tank bottom is

$$h_{c.m.} = R_0\left[\frac{\frac{h}{R_0} + 0.528\beta + 0.128\beta^2\frac{R_0}{h}}{2\left(1 + 0.264\beta\frac{R_0}{h}\right)}\right] \tag{29}$$

Again, h_n depends only on the nth sloshing mode. Also, for $N_{BO} = \infty$, in which case $\Omega_n^2 = \lambda_n$ and $P_{nm} = 0$ for $n \neq m$, equation (27) reduces to $h_n = h - (2R_0/\lambda_n)$, which is the correct result [1]. In every case, the line of action of the spring-mass is slightly nearer the bottom of the tank than for $N_{BO} = \infty$. Since the interest here is primarily in the forces, the results for h_0 and h_n are not presented graphically.

Experimental Results and Comparison With Theory

The main objective of the experimental program was to determine the sloshing force (for incompressible liquids in rigid cylindrical tanks) as a function of the excitation frequency for a frequency band centered about the fundamental mode, with the Bond number being the chief parameter. The apparatus used to accomplish this is shown in Fig. 5; the entire dynamometer-tank-base system is attached directly to the armature of an electrodynamic shaker, which provides the required translational excitation. As can be seen, there are two test tanks (the ones shown are approximately 1 in. dia). One tank, called the active tank, contains the test liquid, and the other tank, called the balance tank, is used to cancel the inertial signal of the empty active tank by appropriate electrical connections of the semiconductor strain gage dynamometer arms and the adding of balance weights; thus the signal recorded is that due only to the inertia of the sloshing liquid.

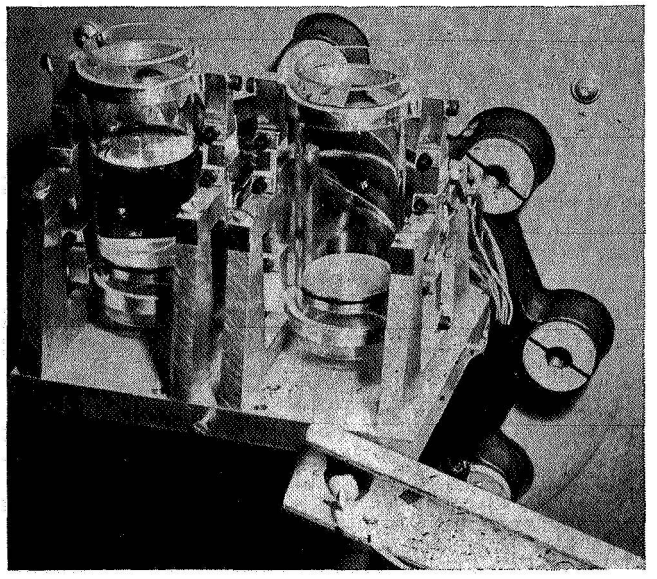

Fig. 5 View of glass tanks and dynamometer

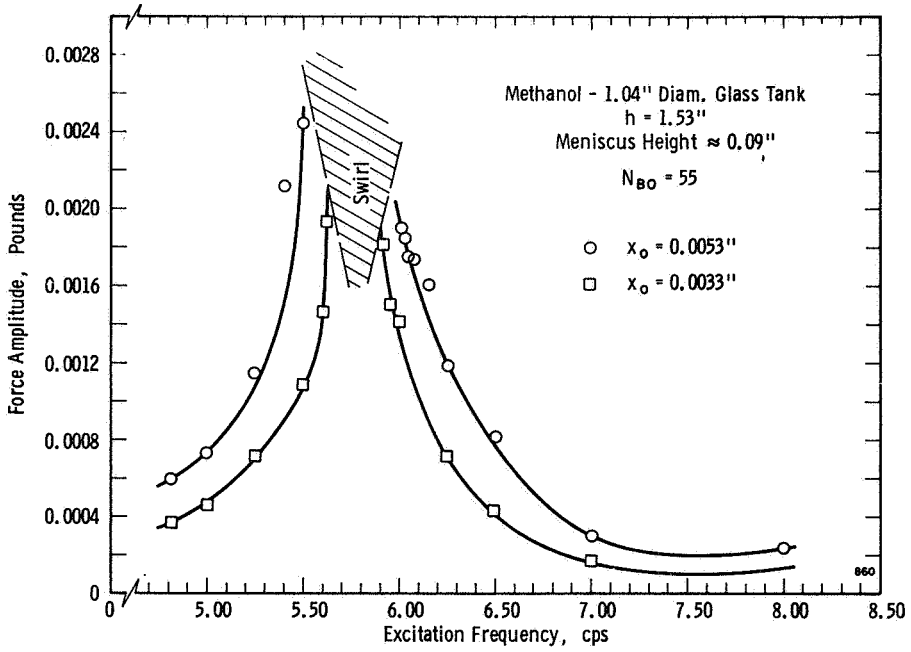

Fig. 6 Force response curve for methanol, Bond number = 55

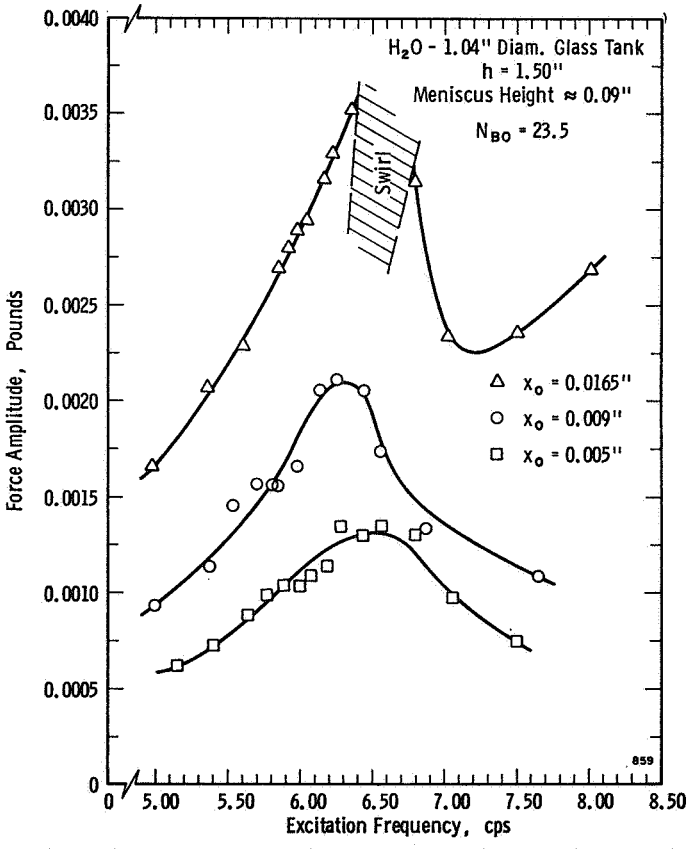

Fig. 7 Force response curve for distilled water, Bond number = 23.5

Four different glass tanks, having diameters ranging from 1.36–0.384 in., were used with three different test liquids: Distilled water, methanol, and carbon tetrachloride. Before each series of tests, the tanks were carefully cleaned in a detergent-and-water solution and rinsed with distilled water. In some of the distilled water tests, the tanks were also cleaned in both a NaOH solution and a hot chromic acid solution. The top of the tank was then covered with a clean plastic wrapper which was removed only to put in the test liquid. The liquids were all reagent grade. In this way, the liquid surface was kept free of contamination.

Figs. 6 and 7 show typical results for methanol and distilled water in a 1.04-in-dia tank. (As nearly as could be determined, the static contact angle of the liquids against the tanks was 0 deg and, except as discussed subsequently, the motion appeared to approximate the "free edge" condition quite well.) The Bond number for the methanol is 55 and, for the water, it is 23.5. The solid lines in these figures are faired curves through the data. There is a pronounced resonance in the methanol curve near 5.75 cps; the curve, in fact, is quite similar to a resonance curve for ordinary high-g sloshing. Near resonance, the sloshing is of the rotary or swirling type encountered in high-g sloshing [13] in which the surface wave rotates around the tank. The shaded areas indicate in a crude fashion the swirl-zone boundaries. Once swirling is encountered, the sloshing force, of course, rotates around the tank also, and thus the forces in this zone cannot be measured nor the exact resonant frequency found.

The water responded in a quite different fashion. The resonance peak is near 6.5 cps instead of the expected value of 5.75 cps. (The theoretical shift in frequency because of the lower N_{BO} of the water is not nearly of this magnitude.) Also, the boundaries of the swirling are displaced upward by a sizable amount and the response curves appear to be heavily damped. Yet, the difference in the viscosity of the water and the methanol (ν_{H_2O} = 1.01 c.s., ν_{meth} = 0.59 c.s.) is not sufficient to explain the variance in the response of the two liquids. Visual observations indicated that the water did not slide freely along the tank walls, even though extreme care was used to prevent contamination of the water and the tanks; as indicated previously, this "sticking" seems to cause additional energy dissipation. Since the interest here is in the "free edge" condition, the response curves for water are not compared to the theoretical predictions.

The experimental value of the natural frequency is determined from the response curves by assuming it is halfway between the swirl boundaries for the lowest excitation amplitude; this is not an exact procedure, but the approximation improves as the width of the swirl region decreases. These values are compared with the present theory in Fig. 8, which also shows the frequency equation of [9]. While there is considerable scatter of the data about the theoretical curve, the general trend of the data and the present theory is in agreement. In fact, except for N_{BO} = 14, the experimental frequencies are below the high-g limit as the theory predicts; and, for several cases, the high-g frequency lies above, i.e., to the right of, the swirl boundaries whereas the true

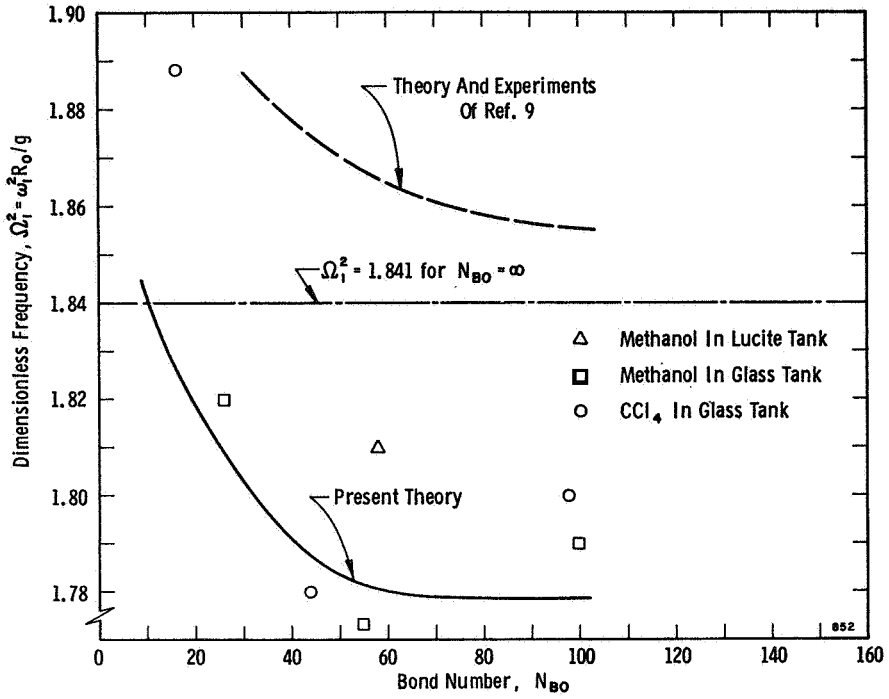

Fig. 8 Comparison of theoretical and experimental natural frequencies for fundamental mode

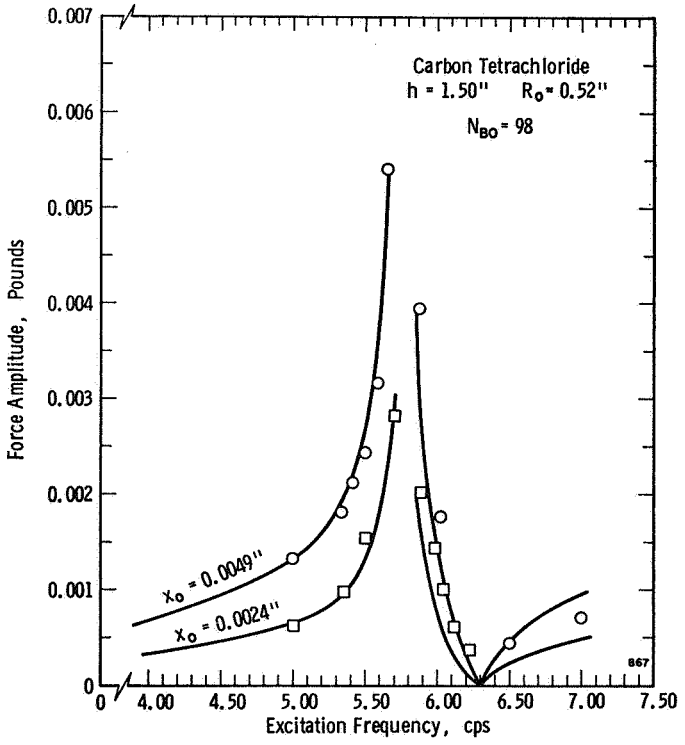

Fig. 9 Comparison of theoretical and experimental force response, $N_{BO} = 98$

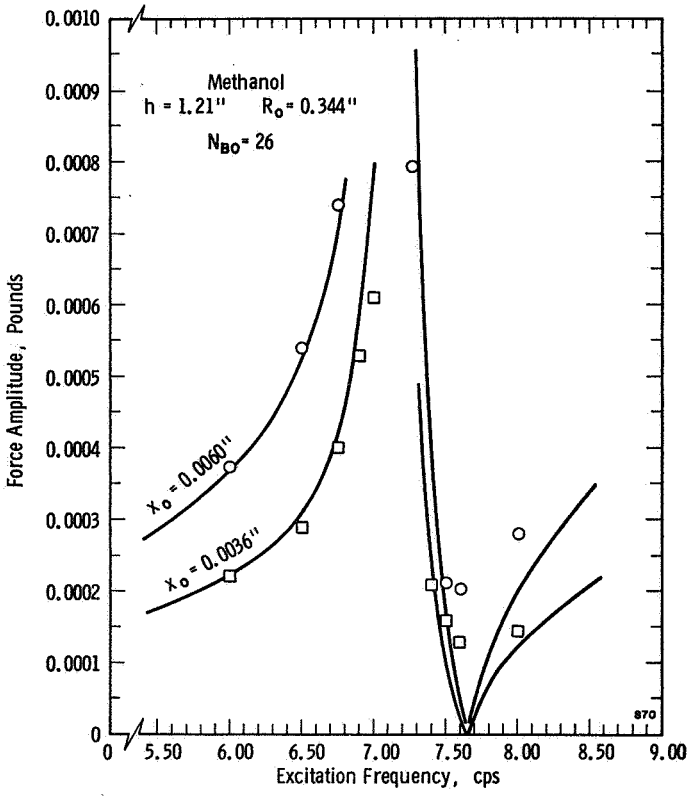

Fig. 10 Comparison of theoretical and experimental force response, $N_{BO} = 26$

natural frequency must lie within the swirl region.

The force response of the proposed mechanical model, with only the fundamental sloshing mass included, is compared with the experimental results in Figs. 9, 10, and 11 for N_{BO} of 98, 26, and 14. (The solid lines in the figures are the theory, and the squares and circles are the experimental data.) The mechanical model and the test results agree very well although there is some discrepancy in the part of the curves above resonance, at least some of which is caused by the influence of higher-order modes neglected in the model. However, for $N_{BO} = 14$ (Fig. 11), there are more serious differences. If the theoretical natural frequency, $f = 9.66$ cps, is used in the model, the predicted forces are generally too large; if the experimental natural frequency, $f = 9.80$ cps, is used, the predicted and the observed forces agree considerably better. It appears, then, that more terms in the velocity potential and wave shape series for $N_{BO} = 14$ need to be retained for proper convergence in the computations.

Conclusions

The analysis shows that the amount of liquid taking part in low-g sloshing is less than that for high-g sloshing. This is a

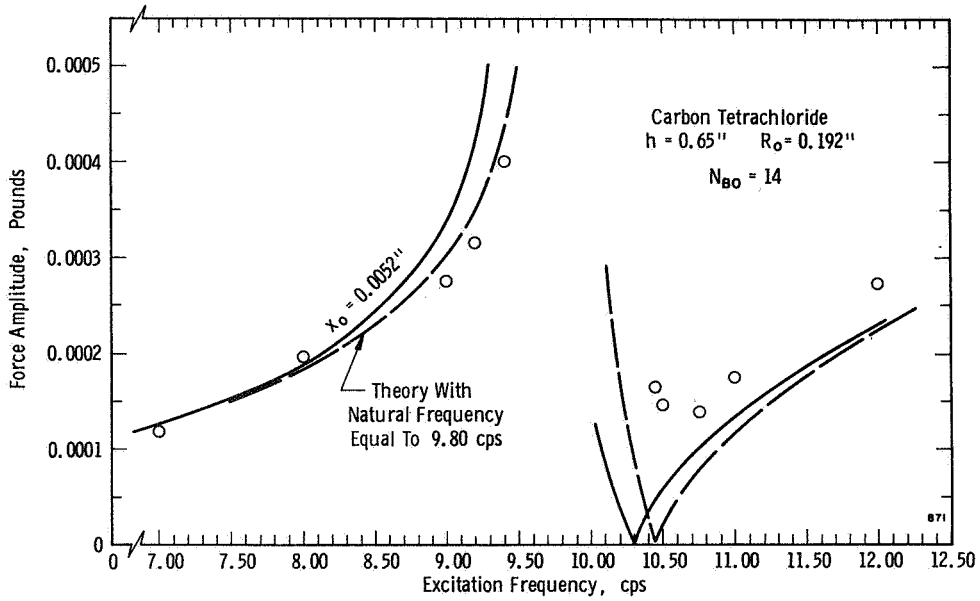

Fig. 11 Comparison of theoretical and experimental force response, N_{BO} = 14

reasonable result because, for the same tank size and the same total amount of contained liquid, more of the liquid is in contact with the walls under low-g conditions; thus more of the liquid must follow the motion of the tank; that is, more of the liquid must be assigned to the rigidly attached mass, m_0, in the mechanical model and less to the sloshing masses. The experimental tests have verified the force response of the proposed mechanical model with about the same degree of accuracy as similar models for high-g sloshing.

The experimental program has demonstrated that it is possible to simulate low-gravity sloshing (i.e., low N_{BO} sloshing) by the use of small models and still get usable results. The amount of damping with such tanks did not appear to be critical. However, care must be used in these kinds of tests to insure that the tanks are very clean and the liquids pure; furthermore, the characteristics of the test liquids and the tank materials should be such as to duplicate the desired conditions of a "free," "partially stuck," or "stuck" contact line.

References

1 Bauer, H. G., "Fluid Oscillations in the Containers of a Space Vehicle and Their Influence Upon Stability," NASA TR R-187, Feb. 1964.

2 Lomen, D. O., "Liquid Propellant Sloshing in Mobile Tanks of Arbitrary Shape," NASA CR-222, Apr. 1965.

3 Abramson, H. N., Chu, W-H., and Dodge, F. T., "Nonlinear Effects in Lateral Sloshing," chapter 3 of *The Dynamic Behavior of Liquids in Moving Containers*, Abramson, H. N., ed., NASA Special Publication SP-106, U. S. Government Printing Office, 1966.

4 Skalak, R., and Yarymovych, M., "Forced Large Amplitude Surface Waves," *Proceedings of the Fourth U. S. National Congress of Applied Mechanics*, ASME, 1962, pp. 1411–1418.

5 Dodge, F. T., Kana, D. D., and Abramson, H. N., "Liquid Surface Oscillations in Longitudinally Excited Rigid Cylindrical Containers," *AIAA Journal*, Vol. 3, No. 4, Apr. 1965, pp. 685–695.

6 Kana, D. D., and Dodge, F. T., "Bubble Behavior in Liquids Contained in Vertically Vibrated Tanks," *Journal of Spacecraft and Rockets*, Vol. 3, No. 5, May 1966, pp. 760–763.

7 Habip, L. M., "On the Mechanics of Liquids in Subgravity," *Astronautica Acta*, Vol. 11, No. 6, 1965, pp. 401–409.

8 Reynolds, W. C., Saad, M. A., and Satterlee, H. M., "Capillary Hydrostatics and Hydrodynamics at Low-G," Technical Report LG-3, Department of Mechanical Engineering, Stanford University, Stanford, Calif., Sept. 1964.

9 Satterlee, H. M., and Reynolds, W. C., "The Dynamics of the Free Liquid Surface in Cylindrical Containers Under Strong Capillary and Weak Gravity Conditions," Technical Report LG-2, Department of Mechanical Engineering, Stanford University, Stanford, Calif., May 1964.

10 Benedikt, E. T., "A Study of Propellant Behavior at Zero Gravity," Final Report, Contract NAS8-11097, North American Aviation, Space and Information Systems Division, Apr. 1966.

11 Ryan, R. S., and Buchanan, H., "An Evaluation of the Low-G Propellant Behavior of a Space Vehicle During Waiting Orbit," NASA TM X-53476, June 1966.

12 Swalley, F. E., Platt, G. K., and Hastings, L. J., "Saturn V Low-Gravity Fluid Mechanics Problems and Their Investigation by Full-Scale Orbital Experiment," *Fluid Mechanics and Heat Transfer Under Low Gravity*, Proceedings of the 1965 Symposium sponsored by USAF-OSR and Lockheed Missiles and Space Co., Cohen, H., and Rogers, M., eds.; no publisher given, pp. 1-1–1-24.

13 Hutton, R. E., "An Investigation of Resonant, Nonlinear Nonplanar Free Surface Oscillations of a Liquid," NASA TN D-1870, May 1963.

14 Miles, J. W., "Damping of Gravity Waves by Surface Films," *Sixth Symposium on Naval Hydrodynamics*, Vol. 2, Paper 23, Washington, D. C., Sept. 1966.

15 Satterlee, H. M., and Chin, J. H., "Meniscus Shape Under Reduced-Gravity Conditions," *Fluid Mechanics and Heat Transfer Under Low Gravity*, Proceedings of the 1965 Symposium sponsored by USAF-OSR and Lockheed Missiles and Space Co., Cohen, H., and Rogers, M., eds.; no publisher given, pp. 13-1–13-24.

16 Dodge, F. T., and Garza, L. E., "Experimental and Theoretical Studies of Liquid Sloshing at Simulated Low Gravities," Technical Report No. 2, Contract NAS8-20290, Southwest Research Institute, San Antonio, Texas, Oct. 1966.

APPENDIX

The constants, or Fourier-Bessel coefficients, in equation (11) and (12) are

$$C1_{nm} = \frac{2\lambda_n^2}{(\lambda_n^2 - 1)[J_1(\lambda_n)]^2} \int_0^1 R \left\{ -\lambda_m J_1(\lambda_m R) + \frac{3\beta R^2}{2(1 - R^3)^{1/2}} J_1'(\lambda_m R) \right\} J_1(\lambda_n R) e^{\lambda_m \beta [1 - (1 - R^3)^{1/2}]} \, dR$$

$$C2_{nm} = \frac{2\lambda_n^2}{(\lambda_n^2 - 1)[J_1(\lambda_n)]^2} \int_0^1 \times R J_1(\lambda_m R) J_1(\lambda_n R) e^{\lambda_m \beta [1 - (1 - R^3)^{3/2}]} \, dR$$

and

$$C3_{nm} = \frac{2\lambda_n^2}{(\lambda_n^2 - 1)[J_1(\lambda_n)]^2} \int_0^1 \frac{R}{(N_{BO})(1 - R^3 + \frac{9}{4}\beta^2 R^4)^{3/2}} \times \left\{ (1 - R^3)^{1/2} \lambda_m^2 J_1(\lambda_m R) + \tfrac{9}{4}\beta^2 R^2 (1 - R^3) J_1(\lambda_m R) + \left[\frac{9\beta^2 R^3 (1 - 0.25R^3)(1 - R^3)^{1/2}}{(1 - R^3 + \frac{9}{4}\beta^2 R^4)^{1/2}} \right] J_1'(\lambda_m R) \right\} J_1(\lambda_n R) dR$$

Reprinted from the September 1967
Journal of Applied Mechanics